PNAS Nexus, 2023, 2, 1–8
https://doi.org/10.1093/pnasnexus/pgad260
Advance access publication 11 August 2023
Research Report

Estimation of natural methane emissions from the largest oil sand deposits on earth

Cao Wei[a,b], Seyed Mostafa Jafari Raad[a] and Hassan Hassanzadeh[a,*]

[a]Department of Chemical and Petroleum Engineering, Schulich School of Engineering, University of Calgary, Calgary, AB T2N 1N4, Canada
[b]State Key Laboratory of Oil and Gas Reservoir Geology and Exploitation, Southwest Petroleum University, Chengdu, Sichuan 610500, China
*To whom correspondence should be addressed: Email: hhassanz@ucalgary.ca
Edited By: Levi Thompson

Abstract

Worldwide methane emission by various industrial sources is one of the important human concerns due to its serious climate and air-quality implications. This study investigates less-considered diffusive natural methane emissions from the world's largest oil sand deposits. An analytical model, considering the first-order methane degradation, in combination with Monte Carlo simulations, is used to quantitatively characterize diffusive methane emissions from Alberta's oil sands formations. The results show that the average diffusive methane emissions from Alberta's oil sands formations is 1.56×10^{-4} kg/m^2/year at the 90th percentile of cumulative probability. The results also indicate an annual diffusive methane emissions rate of 0.857 ± 0.013 Million tons of CO_2e/year (MtCO_2e/year) from Alberta's oil sands formations. This finding suggests that natural diffusive leakages from the oil sands contribute an additional 1.659 ± 0.025 and 5.194 ± 0.079% to recent Canada's 2019 and Alberta's 2020 methane emission estimates from the upstream oil and gas sector, respectively. The developed model combined with Monte Carlo simulations can be used as a tool for assessing methane emissions and current inventories.

Keywords: subsurface methane migration, climate change, greenhouse gases, diffusion, Monte Carlo simulations

Significance Statement

Methane emissions from various industrial sources have garnered significant global attention due to their high radiative forcing contribution to climate change. Additionally, methane reacts with hydroxyl radicals, which play a crucial role in removing other air pollutants; its oxidation also contributes to ozone formation, impacting air quality and posing risks to human, animal, and crop health. This study addresses the often-overlooked diffusive natural methane emissions originating from the largest oil sand deposits on earth. We quantify diffusive methane emissions from Alberta's oil sands. Our findings reveal that methane natural diffusive leakage from oil sands needs to be accounted for in emission assessments.

Introduction

Methane (CH_4) is known as the second most important short-lived greenhouse gas and is 25–34 times more potent than carbon dioxide on a 100-year time horizon and 96 times more potent over a 20-year time horizon (1, 2). Therefore, depending on methane emission rates, the short-term global temperature may increase even if CO_2 emissions decline due to the very long atmospheric lifetime of CH_4 (3). Furthermore, besides the climate change implications, methane also has an air-quality consequence attributed to its reaction with hydroxyl radicals, producing CO and CO_2 (4) and its NO_x-catalyzed ozone formation in the troposphere (5–7). Therefore, a thorough understanding of atmospheric methane emission sources will play a vital role in developing mitigation pathways toward limiting the global average temperature to 2°C above the preindustrial levels (8) and improving air quality.

Recent studies have indicated that human-based activities related to agriculture, oil and natural gas, landfills, and microbial processes in wetlands and waste depositories are the main sources of methane emissions (9–12). Top-down and bottom-up approaches have been widely used to quantify methane emissions. The top-down approach involves measuring changes in atmospheric methane concentration (atmospheric methane emissions) recorded at selected sites and utilizing inverse modeling techniques to estimate the net sink/source of methane at the surface. The commonly used quantification techniques in this approach include the source receptor methods (13), aircraft-based flux

Competing Interest: The authors declare that they have no conflict of interest that could have influenced the work reported in this paper.
Received: February 13, 2023. **Accepted:** July 31, 2023

measurements (14), satellite measurements (15, 16), and hybrid measurement modeling (17, 18). These quantification techniques have been long used in Europe and North America. The bottom-up approach quantifies the emissions based on a methane inventory estimated by provinces/states and local sectors. Discrepancies have always existed between top-down and bottom-up methane emission estimates. The methane emissions measured by a top-down approach are generally greater than bottom-up inventory-based estimates (19–21). This inconsistency is mainly linked to the limited capability of the inventory-based technique to identify all methane emission points from a large number of complex source types (5, 22). The discrepancy has led to the debate that the existing quantifications of methane emissions cannot be broadly accepted. Many studies have indicated that the oil and gas sector leads to this discrepancy, primarily from its production and processing procedures (1). For example, some studies have revealed that the actual methane emission from the oil and gas sectors is higher than the currently reported values (20, 21, 23–25). More specifically, recent studies reported that the airborne measurement-derived emission results were found to be four times greater than the bottom-up inventory-based estimates for the Lloydminster region (26, 27). However, these studies only attributed the discrepancies to anthropogenic methane emissions from the oil and gas sector, such as production, tanks, facilities and equipment, combustion, and bitumen extraction (28–30).

Diffusive natural methane emissions from the oil and gas reservoirs have rarely been studied. This study thus considers natural methane emission escaping from the largest oil sand deposits on earth through diffusion. Methane natural diffusion is a slow upward migration of methane molecules from oil sand deposits through the overlying water-saturated porous layers due to the existing methane concentration gradient. Although diffusion is the slowest transport mechanism, it can be a major factor in depleting the oil and gas accumulations over a geologic time scale (31) and hence it deserves to be considered in methane emissions from oil sand formations. Alberta's oil sands are mainly distributed in the Athabasca, Cold Lake, and Peace River regions, with 168 billion barrels of oil reserves covering an area of 140,000 km^2, as shown in Fig. 1 (32). Alberta's oil sands are mainly hosted within the Wabiskaw–McMurray succession, whose age determined from the microfossil and palynological records is estimated to be ∼125 million years (33). According to kinetic studies, a slow thermal maturation occurs when oil sands are heated under controlled conditions or at the geological formation temperature. The thermal maturation may yield methane, CO_2, CO, H_2S, COS, CS_2, acetaldehyde, and SO_2 (34, 35). A fraction of the generated gases would undoubtedly migrate and escape into the groundwater and atmosphere through diffusion over a geologic time scale (36). Nonetheless, this potential methane emission source type has not been considered in Canada's National Inventory in the recently reported 2020 Methane Emission Management from the Upstream Oil and Gas Sector in Alberta (37).

The aims of this paper are: (i) to present a model to describe the subsurface methane diffusion from oil sands to the surface and thus to the atmosphere; (ii) to provide a zero-order estimate of the methane emission rates from Alberta's oil sands based on the proposed model in combination with Monte Carlo simulations (MCSs); (iii) to calculate the contribution of methane emissions by subsurface diffusion over 140,000 km^2 of Alberta's oil sands to Canada's and Alberta's methane emissions reported from the upstream oil and gas sector, and provide further evidence that allows a more reliable assessment of methane inventory. In addition, the fact that Alberta's oil sands are the largest hydrocarbon deposits on earth (38–40) highlights the importance of considering the global impact of methane emissions from these less-considered sources. Furthermore, this paper addresses a rarely studied methane emission pathway.

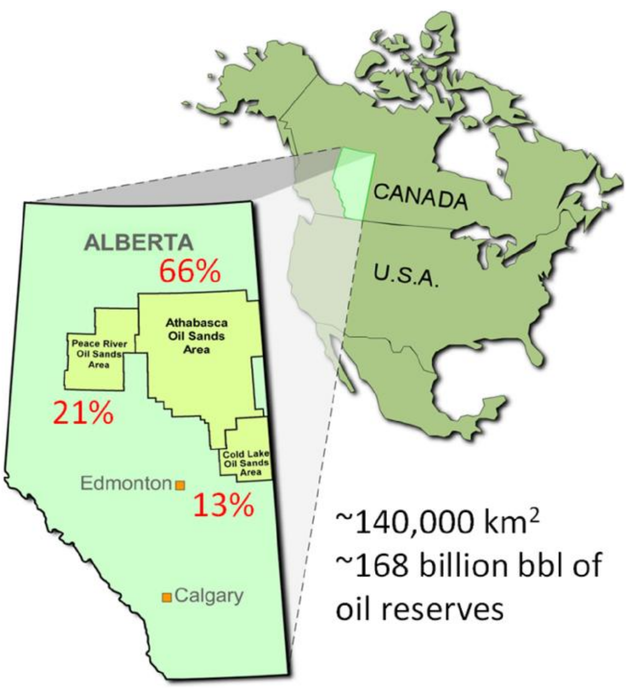

Fig. 1. The Alberta oil sands map (Source: Alberta Geological Service) displays the locations of the Alberta oil sands. Among these, Athabasca, Peace River, and Cold Lake contribute to 66, 21, and 13% of Alberta's oil sands reserves, respectively (32).

Methods

Methane diffusion model

We consider a vertical cross section of a water-saturated porous layer of thickness H overlying the oil sand formation, where $z = 0$ is the top of the oil sand formation and $z = H$ is the earth's surface. The pore water above the oil sand formation is assumed to be stagnant; thus, molecular diffusion is the dominant mechanism in the subsurface methane transport in the water-saturated porous layer. The unsteady-state methane diffusion considering a first-order methane degradation (e.g. oxidation, adsorption, etc.) can be described by:

$$D_{eff}\frac{\partial^2 C_{CH4}}{\partial z^2} - \kappa_d C_{CH4} = \frac{\partial C_{CH4}}{\partial t} \tag{1}$$

with the initial condition (IC):

$$C_{CH4}(z, t = 0) = 0 \tag{2}$$

The oil and pore water are typically saturated with methane at oil sand reservoirs' temperature and pressure (29, 31, 34, 36); thus, the lower boundary condition (BC) at $z = 0$ can be expressed as:

$$C_{CH4}(z = 0, t) = C^*_{CH4} \tag{3}$$

The BC at $z = H$ can be written as:

$$D_{eff}\frac{\partial C_{CH4}}{\partial z} + k_a(C_{CH4} - C^{\infty}_{CH4}) = 0 (z = H, t) \tag{4}$$

where C_{CH4} is the methane concentration in the pore waters (mole/m^3), z is the vertical distance and positive upward, D_{eff} is the effective diffusion coefficient for methane through the water-saturated porous media (m^2/s), t is the time (s), H is the thickness of the water-saturated porous layer/oil sand formation depth (m), κ_d is the degradation constant (s^{-1}), k_a is the mass transfer coefficient across the earth-air interface (m/s), C^{∞}_{CH4} is the surface methane concentration in air, which is set as zero due to its low content in the air, C^*_{CH4} is the dissolved equilibrium concentration of methane in pore waters with a range of 32.9–133.4 mol$_{CH4}$/m$^3_{Aqueous\ phase}$ (41).

The solution of Eq. (1) is obtained by the separation of variables subject to the given IC and BCs. The dimensionless form of the solution is written as:

$$C_{CH4D}(z_D, t_D) = \left(\cosh\sqrt{D_a}z_D - \frac{\left(\sqrt{D_a}\tanh\sqrt{D_a} + D_{sh}\right)}{\sqrt{D_a} + D_{sh}\tanh\sqrt{D_a}}\sinh\sqrt{D_a}z_D\right) + \sum_{n=1}^{\infty} A_n \sin(\mu_n z_D)\cdot e^{-(\mu_n^2 + D_a)t_D} \tag{5}$$

where $C_{CH4D} = C_{CH4}/C^*_{CH4}$, $t_D = D_{eff}t/H^2$, $z_D = z/H$; $D_a = \kappa_d H/D_{eff}$ is the Damköhler number; $D_{sh} = k_a H/D_{eff}$ is the Sherwood number; μ_n is the root of $\mu_n + D_{sh}\tan\mu_n = 0$; and A_n is defined as:

$$A_n = -\frac{2\mu_n(D_{sh}^2 + \mu_n^2)}{(D_a + \mu_n^2)(D_{sh}^2 + \mu_n^2 + D_{sh})} \tag{6}$$

The surface flux of diffusive methane emissions is obtained based on Fick's first law as given by:

$$J_{z_D=1} = -D_{eff}\frac{C^*_{CH4}}{H}\frac{\partial C_{CH4D}}{\partial Z} = D_{eff}\frac{C^*_{CH4}}{H}\left[\left(\frac{D_{sh}\sqrt{D_a}}{D_{sh}\sinh\sqrt{D_a} + \sqrt{D_a}\cos\sqrt{D_a}}\right) - \sum_{n=1}^{\infty}\mu_n A_n\cos(\mu_n)\cdot e^{-(\mu_n^2 + D_a)t_D}\right] \tag{7}$$

where J is the diffusive flux (mole/m^2/s).

Monte Carlo simulations

Like most subsurface geological parameters, many input parameters in Eq. (7) are uncertain for calculating the surface flux of methane emissions. This uncertainty is due to the lack of detailed knowledge of the geological characterizations of the subsurface formations overlying the oil sand deposits. For example, an exact distribution for Alberta's oil sand depth over 140,000 km^2 surface area is not precisely characterized. The depth of oil sand formations can vary from the depth of surface mining operations (<75 m) to the typical depths of in situ thermal recovery operations (~300 m). If only a single value of the oil sand depth (H) is applied for representing the entire Alberta's oil sands, the obtained results could be less meaningful and representative. Other uncertain variables also need the same treatment. In this study, MCS, which has been broadly used in other areas like financial investments, risk management, and geothermal development (42, 43), is introduced to address the uncertainty in the mathematical model parameters. MCS is a statistical experimentation method based on generating a large number of random realizations of a physical problem using a given probability distribution of uncertain variables. In our case, Eq. (7) is used to calculate the surface methane flux during each run of MCS (Supplementary material). The oil sand depth (H), the mass transfer coefficient (k_a), the effective diffusion coefficient (D_{eff}), the dissolved equilibrium concentration of methane in the oil sand pore waters (C^*_{CH4}), and the degradation constant (κ_d) are the probability distribution function parameters used in the MCS. In the following, we introduce the determination of these variables.

Oil sand depth

The depth of oil sand formations can vary from surface pit mining operations (<75 m) to the typical in situ thermal recovery operations depth (~300 m) (29, 44). This study thus focuses on the depth range between 0 and 300 m by assigning a uniform probability distribution reflecting its uncertainty range.

Mass transfer coefficient

We reviewed methane mass transfer coefficients in the air–water interface reported from field and laboratory experiments at different temperatures, as shown in Table 1. The following relationship suggested by Barber et al. (46) can be used to correct the results to obtain the mass transfer coefficient at surface temperature.

$$\frac{k_x}{k_y} = \left(\frac{Sc_x}{Sc_y}\right)^n \tag{8}$$

where k_x is the mass transfer coefficient of the solute at a specified temperature. In this work, the specified temperature equals 2.5°C based on surface temperature statistics in Alberta's five representative municipalities (i.e. Calgary, Edmonton, Fort McMurray, Peace River, and High Level) for nearly 10 years (51). Sc_x is the Schmidt number at the specified temperature obtained from Jähne et al. (52). k_y is the mass transfer coefficient corrected to methane at 20°C ($Sc_y = 620$). n value of −2/3 is used here (46). Eventually, the calculated mass transfer coefficients at Alberta's surface temperature are listed in the last row of Table 1, and this work uses the average value of 0.201×10^{-5} m/s.

Effective diffusion coefficient

Maxwell (53) and Nelson and Simmons (54) defined the effective diffusion coefficient of a solute in a homogeneous water-saturated porous media as:

$$D_{eff} = \frac{\phi^m D}{a} \tag{9}$$

where D is the diffusion coefficient (m^2/s), $\phi = 0.3$ is the porosity, a is the rock texture or tortuosity factor, and m is the lithologic exponent. Following Nelson and Simmons' work (54), a and m equal 1.45 and 1.54, respectively.

Table 1. Experimental mass transfer coefficient of methane in the air at the earth's surface.

Reference	Mass transfer coefficient (10^{-5} m/s)	Temperature (°C)	Schmidt numbers	Mass transfer coefficient at 2.5°C (10^{-5} m/s)
Sebacher et al. (45)	0.47	20	620	0.247
Barber et al. (46)	0.56	20	620	0.294
Schütz et al. (47)	0.17	20	620	0.089
Happell et al. (48)	0.30	20	620	0.157
Cole et al. (49)	0.51	—	600	0.262
Xiao et al. (50)	0.304	—	600	0.156

Table 2. Experimental diffusion coefficient of methane in water.

Reference	Diffusion coefficient (10^{-9} m²/s)	Pressure (MPa)	Temperature (°C)	Diffusion coefficient at 2.5°C, 0.101 MPa (10^{-9} m²/s)	Diffusion coefficient at 10 °C, 3 MPa (10^{-9} m²/s)
Witherspoon and Saraf (55)	1.88	0.101	24.8	0.941	1.220
Wise and Houghton (56)	2.4	0.101	20	1.373	1.782
Gubbins et al. (57)	1.81	0.101	25	0.905	1.174
Tham et al. (58)	1.99	0.101	25	0.995	1.291
Bonoli and Witherspoon (59)	2.38	0.101	40	0.831	1.078
Maharajh and Walkley (60)	1.22	0.101	10	0.942	1.222
Jähne et al. (52)	1.25	0.101	10	0.966	1.252
Sachs (61)	1.4	8.2	25	0.699	0.907
Guo et al. (62)	1.61	5	25	0.804	1.044
Chen et al. (63)	1.44	10	25	0.719	0.933
Bellaire et al. (64)	1.73	0.101	25	0.865	1.122

The methane diffusion coefficients obtained from the reported laboratory and field experiment results at different temperatures and pressures are shown in Table 2. Nelson and Simmons (54) suggested that the diffusion coefficient (D_1) under a specified condition can be estimated from the known conditions (D_0, T_0, μ_0) using the Stokes–Einstein relation, as given by:

$$D_1 = D_0 \frac{T_1}{\mu_1} \frac{\mu_0}{T_0} \tag{10}$$

where D_0 is the known diffusion coefficient under the known absolute temperature T_0 (K) and water viscosity μ_0 (cP), and D_1 is the diffusion coefficient at the specified absolute temperature T_1 (K) and water viscosity μ_1 (cP).

Since the given depth of oil sand ranges from 0 to 300 m, we consider two extreme conditions of 2.5°C and 0.101 MPa for the shallow oil sands and 10°C and 3 MPa (29, 44, 65) for the deep oil sands to obtain the proper range of the diffusion coefficient. The calculated diffusion coefficients of methane in water are listed in the last two rows of Table 2. In this work, we use the average value, ranging from 0.9128×10^{-9} to 1.1841×10^{-9} m²/s, by assigning a uniform probability distribution reflecting its uncertainty.

The dissolved equilibrium concentration of methane in the oil sand pore waters

The oil sands in Athabasca, Cold Lake, and Peace River regions have a gas–oil ratio (GOR) in the range of 4 to 20 standard m³ of methane per 1 m³ of bitumen (41). This GOR range represents a dissolved methane mole fraction range of 0.085 to 0.343 when a typical molar mass of bitumen of 550 g/mole and an oil-specific gravity of 1.005 g/mL are used. Considering the equilibrium constants of the gas–oil ($K_{og} = y^{g}_{CH4}/x^{o}_{CH4}$) and gas–water ($K_{wg} = y^{g}_{CH4}/x^{w}_{CH4}$) systems, the methane partition coefficient for the oil–water system is defined as $\alpha_{wg} = x^{w}_{CH4}/x^{o}_{CH4} \approx 0.007$ (44, 66), resulting in a mole fraction range of 0.0006 to 0.0024 for the dissolved equilibrium concentration of methane in the oil sand pore waters, where y^{g}_{CH4} is the mole fraction of methane in the gas phase, x^{o}_{CH4} and x^{w}_{CH4} are the mole fractions of methane in oil and water, respectively. Therefore, a uniform distribution in the range of 0.0006 to 0.0024 was used in MCS.

Methane degradation constant

Damköhler number varies from 0 to 1 (67). Combining the values of D_{eff} and H and the definition of Damköhler number given in previous sections, the value of degradation constant is obtained as 3.3×10^{-13} s^{-1}.

Results and discussion

An important consideration in MCS is the independency of the results to the number of realizations. Hence, first, the number of realizations necessary to ensure the desired degree of accuracy needs to be determined. In this study, we considered a sufficient number of realizations at which the mean of the surface flux of diffusive methane emissions stabilizes and the coefficient of variance (COV) reduces to an acceptable value, i.e. <0.1 (68). We simulated cases with varying numbers of realizations, ranging from 10^4 to 3×10^8, to identify the minimum number necessary to ensure the convergence of the final solution. The mean and the COV for N realizations are, respectively, defined as (68):

$$\bar{J} = \frac{1}{N} \sum_{i=1}^{N} J_i \tag{11}$$

$$\mathrm{COV} = \frac{1}{\bar{J}} \sqrt{\mathrm{Var}(J)/N} \tag{12}$$

We then plotted the mean of the surface flux of diffusive methane emissions versus the number of realizations (Fig. 2A). As the number of realizations increased, the fluctuation of the mean decreased, and the mean gradually stabilized. We also plotted the COV versus the number of realizations (Fig. 2B). As the number of realizations increased, the COV decreased below 0.1. The results demonstrated in Fig. 2 show that the minimum realization number of $N = 5 \times 10^7$ is required to ensure an independent solution. This work uses the realization number of $N = 10^8$ for conducting MCSs to estimate the surface flux of diffusive methane emissions.

Figure 3 shows the surface methane flux frequency, the corresponding cumulative distribution, and the range distributions of total surface methane emissions from Alberta's oil sands obtained from the MCS with 10^8 realizations. As shown in Fig. 3A, the surface flux of diffusive methane emissions from Alberta's oil sand ranges from 1.41×10^{-6} to 1.41×10^{2} kg/m²/year. The mean/expectation of surface methane emissions through diffusion over 140,000 km² of Alberta's oil sand is $2.449 \pm 0.038 \times 10^{-4}$ kg/m²/year. The uncertainty (S) of 0.038×10^{-4} kg/m²/year is based on the uncertainties of input values and assumptions used in this work, defined as $S = \mathrm{Var}(J)/\sqrt{N}$. Based on the cumulative distribution function shown in Fig. 3B, the cumulative probability of diffusive methane emissions with a surface flux larger

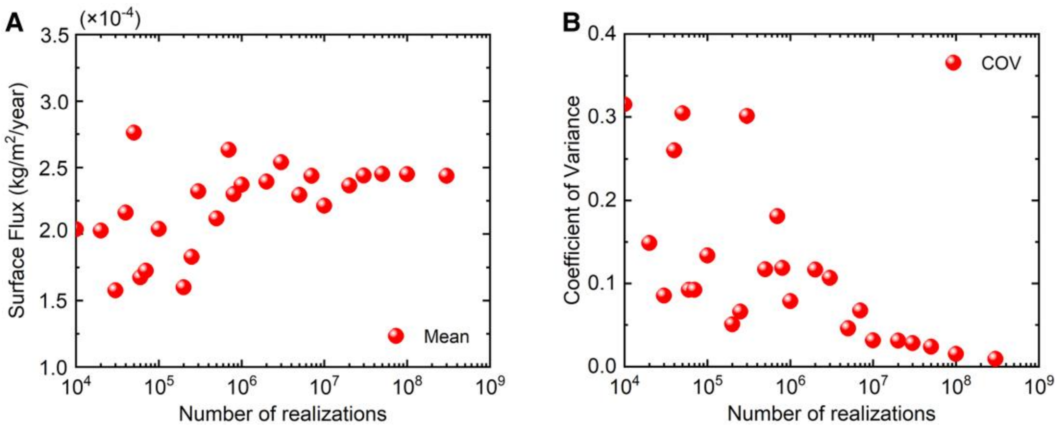

Fig. 2. A) The mean of surface methane flux and B) the coefficient of variance versus the number of realizations.

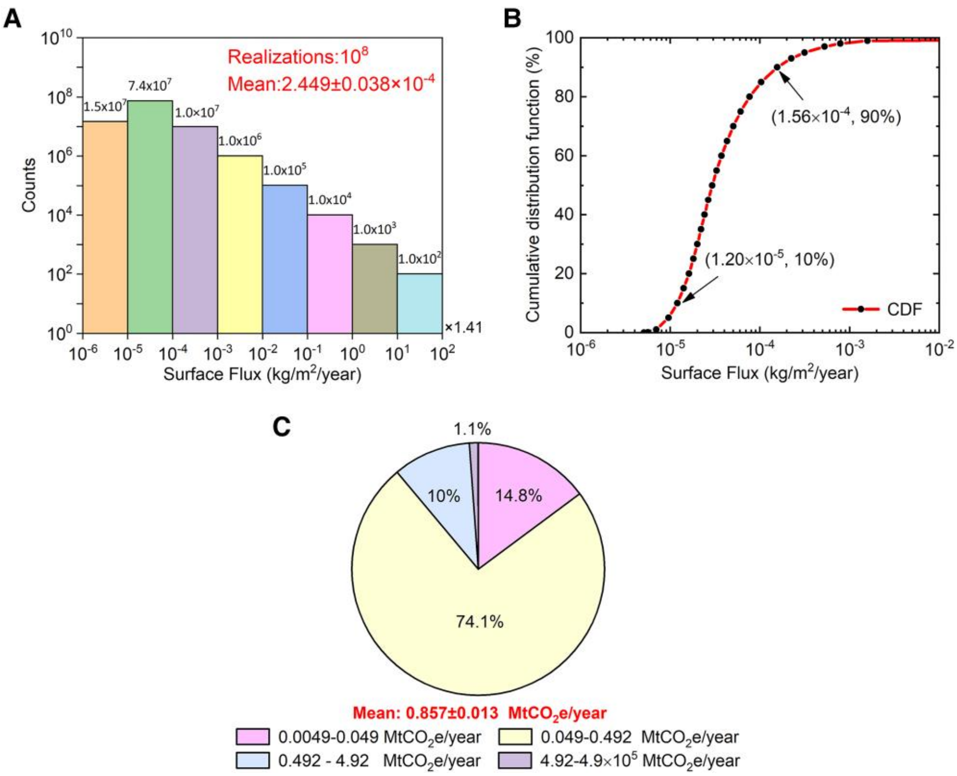

Fig. 3. A) Frequency distribution histogram of surface flux, B) the cumulative distribution function of surface flux, and C) the range distributions of total surface methane emissions with different probability density from Alberta's oil sands generated by MCS with 10^8 realizations. The probability density is obtained using the counts at a given range divided by 10^8 realizations. The mean of surface methane emissions over 140,000 km^2 of Alberta's oil sands is 0.857 ± 0.013 MtCO$_2$e/year.

than 1.20×10^{-5} kg/m^2/year and lower than 1.56×10^{-4} kg/m^2/year is about 80%.

Canada and Alberta have established an equivalency agreement regarding the reduction of methane emissions from the oil and gas sectors (37). International Energy Agency reported that Canada's 2019 methane emissions from the upstream oil and gas sector were 2,066 ktCH$_4$ (69), equivalent to 51.65 MtCO$_2$e/year, using a CH$_4$/CO$_2$ 100-year global warming potential of 25 applied by the Alberta Energy Regulator (37) and Canada's National Inventory Report. According to the government report (2022), Alberta's upstream oil and gas methane emissions were 16.5 MtCO$_2$e in 2020. Alberta's oil sands covered an area of ~140,000 km^2 of the province (Fig. 1). Based on the results of Fig. 3A and C, Alberta's oil sands could release methane to the earth's atmosphere by diffusion with a mean of 0.0343 ± 0.0005 Mt/year, equivalent to 0.857 ± 0.013 MtCO$_2$e/year. The result of 0.857 ± 0.013 MtCO$_2$e/year is $0.857 \pm 0.013/51.65 = 1.659 \pm 0.025\%$ and $0.857 \pm 0.013/16.5 = 5.194 \pm 0.079\%$ of Canada's 2019 and Alberta's 2020 annual methane emission estimates from the upstream oil and gas sector, respectively. Strausz (36) estimated that between 0.1 and 1 Mt/year of volatile hydrocarbons are generated in subsurface Alberta oil sand formations. Our calculation suggests that the methane concentration profile has reached a steady state over geological time. Assuming that a significant fraction of the light hydrocarbons is methane and that most oil sand formations are saturated with methane, the 0.0343 ± 0.0005 Mt/year diffusive flux reveals that a considerable fraction of the generated methane likely remains in the subsurface or degrades in the overlying formations.

Conclusions

This study reports the most probable natural surface flux of methane from the largest oil sand deposits on earth. An analytical model, considering the first-order methane degradation, is developed to study the subsurface methane diffusion. The analytical model is then combined with the MCSs with 10^8 realizations to perform a quantitative analysis of the methane emissions from Alberta's oil sands. It is shown that the most probable surface methane flux range is 1.41×10^{-5} to 1.41×10^{-4} kg/m^2/year. The results show that the most probable surface flux of diffusive methane emissions from Alberta's oil sands is 0.0343 ± 0.0005 Mt/year, equivalent to 0.857 ± 0.013 MtCO$_2$e/year, which would constitute 1.659 ± 0.025 and 5.194 ± 0.079% of Canada's 2019 and Alberta's 2020 inventory-based methane emission estimates from the upstream oil and gas sector, respectively. In addition, the results suggest that a significant fraction of methane generated in oil sand formations most likely remains in the subsurface or degrades in the oil sands overlying geological formations.

More importantly, other oil sands and tar-sand deposits of the world, such as those in Venezuela, the United States, Russia, and China, also cover a large area. The diffusive methane emission results reported here suggest that careful consideration of diffusive methane emissions is necessary to ensure more accurate methane emission estimates globally.

Future research

The analytical analysis of methane diffusion mitigation presented in this work is based on a vertical cross section of a homogeneous water-saturated porous layer overlying oil sand formation. More complex geological features such as formation heterogeneity, lithologies, faults, and fractures can be included to narrow the predicted range of methane diffusive flux. Moreover, the groundwater flow can significantly impact the diffusive flux and the subsurface migration pathways. New theories and techniques should be incorporated to address the role of these complexities, providing a more accurate assessment of diffusive methane emissions from oil sand formations.

Supplementary Material

Supplementary material is available at *PNAS Nexus* online.

Funding

The authors acknowledge the financial support of the Natural Sciences and Engineering Research Council of Canada and member companies of SHARP Research Consortium. The support of the Department of Chemical and Petroleum Engineering and the Schulich School of Engineering at the University of Calgary is also acknowledged. C.W. thanks the China Scholarship Council for supporting his fellowship to study at the University of Calgary, Alberta, Canada (No.202106440056).

Author Contributions

C.W.: Conceptualization, data curation, formal analysis, investigation, methodology, validation, visualization, writing original draft, writing—review and editing. S.M.J.R.: Conceptualization, data curation, formal analysis, investigation, methodology, validation, supervision, writing—review and editing. H.H.: Conceptualization, formal analysis, validation, supervision, methodology, writing—review and editing, funding acquisition.

Data availability

All data used in the MCSs are reported in the main text of this paper. The MATLAB code used in this work for the analytical solution and MCSs is provided as supplementary material.

References

1 Chan E, *et al.* 2020. Eight-year estimates of methane emissions from oil and gas operations in western Canada are nearly twice those reported in inventories. *Environ Sci Technol.* 54:14899–14909.
2 Gasser T, *et al.* 2017. Accounting for the climate–carbon feedback in emission metrics. *Earth Syst Dyn.* 8:235–253.
3 Alvarez RA, Pacala SW, Winebrake JJ, Chameides WL, Hamburg SP. 2012. Greater focus needed on methane leakage from natural gas infrastructure. *Proc Natl Acad Sci USA.* 109:6435–6440.
4 Vaghjiani GL, Ravishankara AR. 1991. New measurement of the rate coefficient for the reaction of OH with methane. *Nature.* 350:406–409.
5 Baray S, *et al.* 2018. Quantification of methane sources in the Athabasca Oil Sands Region of Alberta by aircraft mass balance. *Atmospheric Chem Phys.* 18:7361–7378.
6 Pinto J. 2009. Wyoming Winter smog. *Nat Geosci.* 2:88–89.
7 Schnell RC, *et al.* 2009. Rapid photochemical production of ozone at high concentrations in a rural site during winter. *Nat Geosci.* 2: 120–122.
8 UNFCCC. The Paris Agreement | UNFCCC [accessed 2020 Apr 1]. https://unfccc.int/process-and-meetings/the-paris-agreement/the-paris-agreement.
9 Bazhin N. 2010. Theory of methane emission from wetlands. *Energy Environ Sci.* 3:1057.
10 Metya A, *et al.* 2022. Methane sources from waste and natural gas sectors detected in Pune, India, by concentration and isotopic analysis. *Sci Total Environ.* 842:156721.
11 Nelson B, Zytner RG, Dulac Y, Cabral AR. 2022. Mitigating fugitive methane emissions from closed landfills: a pilot-scale field study. *Sci Total Environ.* 851:158351.
12 Zhang Z, *et al.* 2017. Emerging role of wetland methane emissions in driving 21st century climate change. *Proc Natl Acad Sci USA.* 114:9647–9652.
13 McLaren R, *et al.* 1996. Real-world measurements of exhaust and evaporative emissions in the Cassiar tunnel predicted by chemical mass balance modeling. *Environ Sci Technol.* 30:3001–3009.
14 Mays KL, *et al.* 2009. Aircraft-based measurements of the carbon footprint of Indianapolis. *Environ Sci Technol.* 43:7816–7823.
15 Jacob DJ, *et al.* 2016. Satellite observations of atmospheric methane and their value for quantifying methane emissions. *Atmospheric Chem Phys.* 16:14371–14396.
16 Turner AJ, *et al.* 2016. A large increase in U.S. methane emissions over the past decade inferred from satellite data and surface observations. *Geophys Res Lett.* 43:2218–2224.
17 Allen D. 2004. Evaluation of pollutant outflow and CO sources during TRACE-P using model-calculated, aircraft-based, and

measurements of pollution in the troposphere (MOPITT)-derived CO concentrations. *J Geophys Res*. 109:D15S03.
18 Shephard MW, *et al*. 2015. Tropospheric emission spectrometer (TES) satellite observations of ammonia, methanol, formic acid, and carbon monoxide over the Canadian oil sands: validation and model evaluation. *Atmospheric Meas Tech*. 8:5189–5211.
19 Allen DT, *et al*. 2022. A Methane Emission Estimation Tool (MEET) for predictions of emissions from upstream oil and gas well sites with fine scale temporal and spatial resolution: model structure and applications. *Sci Total Environ*. 829:154277.
20 Brandt AR, *et al*. 2014. Methane leaks from North American natural gas systems. *Science*. 343:733–735.
21 Miller SM, *et al*. 2013. Anthropogenic emissions of methane in the United States. *Proc Natl Acad Sci USA*. 110:20018–20022.
22 Riddick SN, Mauzerall DL. 2023. Likely substantial underestimation of reported methane emissions from United Kingdom upstream oil and gas activities. *Energy Environ Sci*. 16:295–304.
23 Barkley ZR, *et al*. 2019. Forward modeling and optimization of methane emissions in the South Central United States using aircraft transects across frontal boundaries. *Geophys Res Lett*. 46: 13564–13573.
24 Chambers AK, Strosher M, Wootton T, Moncrieff J, McCready P. 2008. Direct measurement of fugitive emissions of hydrocarbons from a refinery. *J Air Waste Manag Assoc*. 58:1047–1056.
25 Karion A, *et al*. 2013. Methane emissions estimate from airborne measurements over a western United States natural gas field. *Geophys Res Lett*. 40:4393–4397.
26 Johnson MR, Tyner DR, Conley S, Schwietzke S, Zavala-Araiza D. 2017. Comparisons of airborne measurements and inventory estimates of methane emissions in the Alberta upstream oil and gas sector. *Environ Sci Technol*. 51:13008–13017.
27 O'Connell E, *et al*. 2019. Methane emissions from contrasting production regions within Alberta, Canada: implications under incoming federal methane regulations. *Elem Sci Anthr*. 7:3.
28 Lyon DR, *et al*. 2016. Aerial surveys of elevated hydrocarbon emissions from oil and gas production sites. *Environ Sci Technol*. 50: 4877–4886.
29 Mohammadi M, Jafari Raad SM, Zirrahi M, Hassanzadeh H. 2021. Subsurface migration of methane from oil sands thermal recovery operations. *Water Resour Res*. 57:e2020WR028745.
30 Small CC, Cho S, Hashisho Z, Ulrich AC. 2015. Emissions from oil sands tailings ponds: review of tailings pond parameters and emission estimates. *J Pet Sci Eng*. 127:490–501.
31 Smith JE, Erdman JG, Morris DA. 1971. Migration, accumulation and retention of petroleum in the earth. Paper presented at the 8th World Petroleum Congress, Moscow, USSR.
32 Government of Alberta. 2022. The Location of Oil Sands—Oil Sands [accessed 2023 Aug 8]. http://history.alberta.ca/energyheritage/sands/origins/the-geology-of-the-oil-sands/the-location-of-oil-sands.aspx.
33 Hein FJ, Dolby G. 2018. Lithostratigraphy, palynology, and biostratigraphy of the Athabasca oil sands deposit, northeastern Alberta: Alberta Energy Regulator. AER/AGS Open File Report 2017–08 (105 pp.).
34 Hassanzadeh H, Harding TG, Moore RG, Mehta SA, Ursenbach MG. 2016. Gas generation during electrical heating of oil sands. *Energy Fuels*. 30:7001–7013.
35 Vitt DH, Halsey LA, Bauer IE, Campbell C. 2000. Spatial and temporal trends in carbon storage of peatlands of continental western Canada through the Holocene. *Can J Earth Sci*. 37:683–693.
36 Strausz OP, Mojelsky TW, Lown EM. 1977. *The chemistry of the Alberta oil sand bitumen*. Edmonton: Hydrocarbon Research Center, Department of Chemistry, University of Alberta.
37 Government of Alberta. 2022. Methane Emissions Management from the Upstream Oil and Gas Sector in Alberta—Open Government [accessed 2022 Jun 30]. https://open.alberta.ca/publications/methane-emissions-management-upstream-oil-and-gas-sector#summary.
38 Chilingarian GV, Yen TF, editors. 1978. *Bitumens, asphalts, and tarsands*. New York: Elsevier Scientific Publishing Co.
39 Speight JG. 2013. *Oil sand production processes*. Oxford: Gulf Professional Publishing.
40 CAPP. 2022. What Are the Oil Sands | Canada's Oil Sands Facts & Information. n.d. [Retrieved 2022 Oct 16]. https://www.capp.ca/oil/what-are-the-oil-sands/.
41 Al-Gawfi A, Zirrahi M, Hassanzadeh H, Abedi J. 2019. Development of generalized correlations for thermophysical properties of light hydrocarbon solvents (C_1–C_5)/bitumen systems using genetic programming. *ACS Omega*. 4:6955–6967.
42 Rajasekhar B, Nambi IM, Govindarajan SK. 2018. Human health risk assessment of ground water contaminated with petroleum PAHs using Monte Carlo simulations: a case study of an Indian metropolitan city. *J Environ Manage*. 205:183–191.
43 Walstrom JE, Mueller TD, McFarlane RC. 1967. Evaluating uncertainty in engineering calculations. *J Pet Technol*. 19:1595–1603.
44 Jafari Raad SM, Hassanzadeh H. 2022. Subsurface containment of injected chemicals during in-situ bitumen recovery from oil sands. *ACS EST Eng*. 2:681–688.
45 Sebacher DI, Harriss RC, Bartlett KB. 1983. Methane flux across the air-water interface: air velocity effects. *Tellus B*. 35B:103–109.
46 Barber TR, Burke RA, Sackett WM. 1988. Diffusive flux of methane from warm wetlands. *Glob Biogeochem Cycles*. 2:411–425.
47 Schütz H, Conrad R, Goodwin S, Seiler W. 1988. Emission of hydrogen from deep and shallow freshwater environments. *Biogeochemistry*. 5:295–311.
48 Happell JD, Chanton JP, Showers WJ. 1995. Methane transfer across the water-air interface in stagnant wooded swamps of Florida: evaluation of mass-transfer coefficients and isotropic fractionation. *Limnol Oceanogr*. 40:290–298.
49 Cole JJ, Bade DL, Bastviken D, Pace ML, Van de Bogert M. 2010. Multiple approaches to estimating air-water gas exchange in small lakes: gas exchange in lakes. *Limnol Oceanogr Methods*. 8: 285–293.
50 Xiao S, *et al*. 2014. Gas transfer velocities of methane and carbon dioxide in a subtropical shallow pond. *Tellus B Chem Phys Meteorol*. 66:23795.
51 Government of Canada. 2022. Alberta—Weather Conditions and Forecast by Locations—Environment Canada [accessed 2020 Jun 30]. https://weather.gc.ca/forecast/Canada/index_e.html?id=AB.
52 Jähne B, Heinz G, Dietrich W. 1987. Measurement of the diffusion coefficients of sparingly soluble gases in water. *J Geophys Res*. 92: 10767.
53 Maxwell JC. 1873. *A treatise on electricity and magnetism*. New York: Clarendon Press.
54 Nelson JS, Simmons EC. 1995. Diffusion of methane and ethane through the reservoir cap rock: implications for the timing and duration of catagenesis. *AAPG Bull*. 79:1064–1073.
55 Witherspoon PA, Saraf DN. 1965. Diffusion of methane, ethane, propane, and n-butane in water from 25 to 43°. *J Phys Chem*. 69: 3752–3755.
56 Wise DL, Houghton G. 1966. The diffusion coefficients of ten slightly soluble gases in water at 10–60°C. *Chem Eng Sci*. 21: 999–1010.
57 Gubbins KE, Bhatia KK, Walker RD. 1966. Diffusion of gases in electrolytic solutions. *AIChE J*. 12:548–552.

58 Tham MJ, Bhatia KK, Gubbins KF. 1967. Steady-state method for studying diffusion of gases in liquids. *Chem Eng Sci*. 22:309–311.

59 Bonoli L, Witherspoon PA. 1968. Diffusion of paraffin, cycloparaffin and aromatic hydrocarbons in water and some effects of salt concentration. In: Schenck PA, Havennar I, editors. *Advances in organic geochemistry* 1968. New York: Pergamon. p. 373–384.

60 Maharajh DM, Walkley J. 1973. The temperature dependence of the diffusion coefficients of Ar, CO_2, CH_4, CH_3 Cl, CH_3 Br, and $CHCl_2$ F in water. *Can J Chem*. 51:944–952.

61 Sachs W. 1998. The diffusional transport of methane in liquid water: method and result of experimental investigation at elevated pressure. *J Pet Sci Eng*. 21:153–164.

62 Guo H, Chen Y, Lu W, Li L, Wang M. 2013. In situ Raman spectroscopic study of diffusion coefficients of methane in liquid water under high pressure and wide temperatures. *Fluid Phase Equilib*. 360:274–278.

63 Chen YA, *et al*. 2018. Measurements of diffusion coefficient of methane in water/brine under high pressure. *Terr Atmospheric Ocean Sci*. 29:577–587.

64 Bellaire D, Großmann O, Münnemann K, Hasse H. 2022. Diffusion coefficients at infinite dilution of carbon dioxide and methane in water, ethanol, cyclohexane, toluene, methanol, and acetone: a PFG-NMR and MD simulation study. *J Chem Thermodyn*. 166:106691.

65 Wei C, Nawaz A, Nath D, Zirrahi M, Hassanzadeh H. 2022. Subsurface waste heat recovery from the abandoned steam assisted gravity drainage (SAGD) operations. *Energy*. 256:124615.

66 Zirrahi M, Azin R, Hassanzadeh H, Moshfeghian M. 2012. Mutual solubility of CH_4, CO_2, H_2S, and their mixtures in brine under subsurface disposal conditions. *Fluid Phase Equilib*. 324:80–93.

67 Sabet N, *et al*. 2020. Numerical modeling of viscous fingering during miscible displacement of oil by a paraffinic solvent in the presence of asphaltene precipitation and deposition. *Int J Heat Mass Transf*. 154:119688.

68 Johnson PA. 1992. Reliability-based pier scour engineering. *J Hydraul Eng*. 118:1344–1358.

69 Methane Tracker Data Explorer—Data Tools—IEA. (n.d.). [Retrieved 2022 Oct 16]. https://www.iea.org/data-and-statistics/data-tools/methane-tracker-data-explorer.